

EXPERIMENTAL STUDY OF VORTEX EFFECTS ON A FIGHTER AIRCRAFT FOREBODY AT HIGH ANGLE OF ATTACK

K. Widing

The Aeronautical Research Institute of Sweden (FFA), Bromma, Sweden

Abstract

Low speed wind tunnel investigations of a fighter aircraft forebody at high angle of attack and sideslip have been carried out. With the intention to simplify the complex flow situation it was decided to work with part-models of the aircraft forebody. The main purpose was to study the Re-number effects by testing at various free stream velocities but also by using different model scales. The test programme included force and pressure measurements and also oil flow tests to visualize the boundary layer flow on the surface of the forebody.

The investigation has shown that the flow is extremely sensitive to the Re-number and very pronounced differences have been found with different models even at the same Re-number. Furthermore, it has been found that active directional control of the aircraft by use of different forebody add-on devices appears promising. This initial investigation will be followed by further work to improve knowledge concerning the flow problems involved.

I. Introduction

For modern high-performance fighter aircraft the requirements of combat agility have emphasized the need for controlled flight at extremely high angles of attack. In this regime unsymmetric separated vortex flow from the forebody can develop large side forces and yawing moments even at zero sideslip angles.

For the new Swedish fighter, the JAS 39 "Gripen", the wind tunnel investigation programme accordingly included tests at high angles of attack. The main purpose was to study the future development potential towards enlargement of the flight regime. The chosen model scale, 1:6.5, for the low speed wind tunnel investigations meant that FFA's 3.6 m dia. low speed wind tunnel (because of tunnel wall interference) was too small for tests at the high angles of attack under consideration. Therefore, the main part of the low speed programme was carried out in large tunnels abroad.

Those test showed that the flow as expected was very sensitive to Re-number and that transition trips had significant effects. The unsymmetrical flow over

the forebody, both concerning more or less gradual transition and separated areas, generates locally unsymmetric loads. The flow separations, in form of intense unsymmetric vortices, affect the rest of the flow around the aircraft e.g. the flow over the wings and the fin. This makes it difficult from balance test results to judge in detail how the vortex flow locally affects the aircraft. It has been clearly documented that a large part of the loads originates from the forebody. In an attempt to make it easier to approach the problems and to be able to study the flow phenomena in more detail subsequent tests were carried out with part-models of the aircraft forebody.

II. Model Description

Figure 1 shows the part of the aircraft, about 36% of the length, of which models were build. Notice that both the canard wings and the air intakes are excluded.

Two forebody models of different sizes were designed and manufactured for tests in the low speed wind tunnel at FFA. To reach as high Re-number as possible the scale of the larger one was chosen to be 1:2.5, which is about the biggest suitable with respect to wind tunnel blockage. The smaller one is in the scale 1:6.5, which is the same scale as the full model. The large and the small models were denoted L and S, respectively.

Figure 1 also shows the main dimensions of the large model. The models were equipped with an internal six-component balance to measure the forces and moments on the forward part of the model. Both models are equipped with 212 pressure tappings distributed around 14 cross sectional stations along the model, according to Figure 2. The tappings are connected to 6 Scanivalve pressure blocks situated inside the model.

Some of the tests with model S were carried out with transition trips. The configuration was equipped with ten rows of tape strips equally spaced over the forebody, according to Figure 3.

III. Wind Tunnel Installation

The tests were conducted in FFA's low speed wind tunnel, which is a continuous closed - circuit wind tunnel with a 3.6 m circular test section and a maximum velocity of 83 m/s. For these tests a special high- α rig is used. Figure 4 shows the large model installed in the tunnel and Figure 5 shows the rig arrangements. The model is sting-mounted and connected by an arm to a turntable, which permits angles of attack in the range of $\pm 90^\circ$. Rotating the model gives sideslip conditions.

IV. Test Programme

The angle of attack range was from 0 to 90 degrees and the angle of sideslip range was from -20 to +20 degrees. The sideslip series were run at $\alpha=40, 50, 60, 70$ and 80 degrees. The models were tested at various speeds in the range from 22 to 58 m/s. The highest speed with the large model (1:2.5) gives a maximum Re-number of 6.9 million based on the mean aerodynamic chord. When running the large model at 22 m/s and the small model (1:6.5) at 58 m/s the Re-numbers are equal — 2.6 million.

V. Configurations

During the testing periods with these two models a number of different configurations have been investigated. Only a few according to the list, Figure 6, can be treated in this paper. Starting from a basic configuration simply consisting of a bare cone with a rotational symmetric tip, different devices have been added. Configuration 2 is characterized by the pitot-tube. Configuration 3 is equipped with two horizontal strakes. On configuration 4 the starboard strake is retracted. Figure 7 gives the main dimensions of the add-on devices.

VI. Results and discussion

First some results from the tests with the large model are treated showing Re-number sensitivities for the different configurations and also the effects of the add-on devices.

Secondly results from tests with both the large and the small model are compared, which of course give further information of the Re-number dependence of the configurations.

Thirdly the effects of transition trips on the small part-model for three configurations are shown.

Model L. Configuration 1

Initial α -series with conf. 1 showed that the configuration was extremely sensitive to variations of the wind tunnel speed e.g. Re-number, which is evident from Figure 8. Here the variations with angle of attack of the five components C_N, C_m, C_C, C_n and C_l are shown. Generally the normal force and the pitching moment vary slightly with configuration changes. The rolling moment is small. The yawing moment shows about the same behaviour as the sideforce. From here on only the sideforce variations with angle of attack and sideslip are presented.

The effects of sideslip at $\alpha=40^\circ$ and below are as a rule small and are also excluded in this presentation. Figure 9 shows the results for $\alpha=50^\circ, 60^\circ$ and 70° at 22 and 58 m/s. Again significant differences are found at the two velocities. The series were run from -20° to $+20^\circ$ and back again and despite large and abrupt sideforce changes only minor hysteresis effects have been noticed.

The flow conditions at some specific angle of attack have been studied by oil flow tests. Figure 10 shows the perfect symmetric flow with no sideforce at $\alpha=40^\circ$. The maximum sideforce at 58 m/s was obtained at $\alpha=62^\circ$. Figure 11 shows considerable differences concerning the transition and separation lines on the two sides of the forebody. To establish the transition line more clearly evaporation tests were also carried out, the lower photo. The lines from the oil flow and the evaporation tests coincide very well.

From all the pressure measurements it has been decided to show some results at this maximum sideforce case, $\alpha=62^\circ$, and at different free stream velocities. In Figure 12 the C_p -values have been plotted on every other pressure measuring station. The vector sums of the pressure forces are also included in the figures as straight lines. It can be seen that on the front of the model there are pressure distribution variations along the body but that the local loads all point towards the right corresponding to positive sideforces. On the aft part, however, the loads successively change directions decreasing the total sideforce.

The most marked effects of velocity variations occurs at $\alpha=76^\circ$. Figure 13 shows two completely different flows where e.g. the trace of a vortex separation has shifted from the port side at 58 m/s to the starboard side at 22 m/s.

Model L. Comparison of Configurations 1 and 2. The effects of the pitot-tube

The differences between the sideforces of these configurations are really significant. Conf. 2, Figure 14, shows major improvements both concerning the angle of attack and sideslip behaviour. Adding the pitot-tube means that the sideforces become close to

zero in the entire α -regime from 0° to 90° at $\beta = 0^\circ$ and at both 58 and 22 m/s. As the oil flow picture shows, the boundary layer flow on the forebody, Figure 15, is also nearly symmetric. On the close-up it can be observed that the pitot-tube vortex separation lines pass into the corresponding separation of the tip of the nose. Maybe this flow mechanism is essential for developing the symmetric and very stable flow over the forebody.

Model L. Comparison of Configurations 2 and 3. The effects of the two short strakes

Figure 16 shows that adding the two strakes to a pitot-tube equipped nose effects the sideforce only slightly. But there are no major differences between the results at 22 and 58 m/s. The configuration appears to be insensitive to Re-number.

Model L. Comparison of Configurations 3 and 4. The effects of retracted starboard strake

Here the objective is to study the possibility of contributing to the directional control of the aircraft by retraction of one of the strakes. Figure 17 shows that in large α -intervals it gives very pronounced sideforces. The initial sideforce (at $\beta=0^\circ$) that can be applied is shown by the α -curves in the figure. At 58 m/s an abrupt sign shift can be seen. The retraction of the starboard strake gives a sideforce towards starboard for angles up to about 56° but at higher angles the effects are reversed. The retraction of a strake can also be used to give a returning sideforce on a sideslip disturbance. Figure 18 shows at 58 and 22 m/s the available ΔC_C at a sideslip angle of $+10^\circ$ and also the accompanying sign shift. Furthermore, from both the α - and β -series it is obvious that the effects when compared to the results at 22 and 58 m/s are very Re-number dependent.

As mentioned earlier the low speed test programme for the "JAS" was carried out with a full model in the scale 1:6.5. Some results from those tests are shown in Figure 19. The forebody configuration was identical to conf. 2 of this paper e.g. a pitot-tube equipped nose. The figure shows in fact the yawing moment but the main part of it is assumed to be caused by sideforce loads on the forebody. The tests were run at Re-numbers of 2.8 and 7.7 million (a pressurized wind tunnel) and were done with and without transition tripping. The results may in principle be compared with those of Figure 14 where 58 m/s corresponds to a Re-number of 6.9 million and 22 m/s to 2.6 million. Despite Re-numbers of the same order the trends of the results are remarkably different. The symmetric flow over the part-model is obviously replaced by a pronounced asymmetric one in the full model case. The results from the full model are similar to those obtained with the configuration without pitot-tube (conf. 1), Figure 8.

The "JAS" prototypes now flying are equipped with a pair of strakes and consequently do not experience these asymmetries so the results shown are not valid for the aircraft. But still the knowledge of the very explicit Re-number dependence is important especially if in a future increase of the α -range efforts are made to control the aircraft by use of the forces available on the forebody.

The work so far has shown amongst other things that configuration changes at 22 and 58 m/s give different results and that the part model (1:2.5) does not show the same characteristics as the full model. Those were the main reasons, together with the need for improved understanding of the flow phenomena, for the decision to build and test a smaller part-model in the same scale as the full model — 1:6.5.

Model S. Without transition trips

The same test programme was carried out for this smaller part-model as for the larger one. Only some typical results from the α -series ($\beta=0^\circ$) and β -series at $\alpha=60^\circ$ and 70° are presented here. For the same four configurations, 1 to 4, as investigated earlier, the sideforces obtained are shown in Figure 20 to 23. Here the results from the large model at 22 m/s and the small model at 58 m/s i.e. at the same Re-number, 2.6 million, are compared. Also included in the graphs are the results at the highest available Re-number, 6.9 million (the large part-model at 58 m/s). For both α - and β -series, conf. 2 (pitot-tube), Figure 21, is least influenced by changes in Re-number. Conf. 3 (two strakes), Figure 22, shows considerable differences at sideslip conditions. For conf. 1 (bare nose), Figure 20, and conf. 4 (port strake), Figure 23, the results show tremendous differences both concerning the α - and β -series. The troublesome fact is that these results have been obtained despite geometrical identical models (but at different scale) tested at the same Re-number.

Model S. With transition trips

The common method when dealing with low Re-number problems to force transition by use of trips has also been used here with the small part-model. The results in the previous section for the model without transition trips produced for the Re-number studies also serves here as a base for establishing the effects of the transition trips. A number of different trip configurations have been tested but the results from just one of them are presented according to Figure 3. Three of the configurations tested earlier — 1, 2 and 3 — were equipped with transition trips and the results are shown in Figures 24, 25, 26 respectively. For comparison, the results from the large model are included in the graphs as before. In general this transition trip configuration has a pronounced influence on the flow. The α -series in Figure 24 — conf. 1 — shows for example that the sideforces have the same trend as

obtained with the large model and the forces have increased between $\alpha = 50^\circ$ and 65° to the same level. The α -series in Figure 25 are especially interesting because here the trips have created unsymmetric flow conditions. Unsymmetric conditions were also found at the high Re-number tests discussed earlier (Figure 19). Figure 26 shows the relatively small transition trip effects with configuration 3.

VII. Concluding remarks

It has been a major advantage to work with part-models because of the possibilities of the direct coupling between the measured forces and the boundary layer flow observed on the forebody. There are so far no indications that the part-model approach means that basic information concerning the forebody loads is lost. The variations brought about on the one hand by changes of the free stream velocities and on the other by different model scales showed that the flow is extremely sensitive to the Re-number. Furthermore, despite having the same Re-number considerable differences concerning the loads on the forebody were found for different models.

The transition trip configuration chosen for the small part-model affects the results differently depending on the model configuration. There are cases where the trips have created a high Re-number unsymmetric flow from a former low Re-number symmetric one. The investigations with add-on devices indicate promising results. It was noticed that even those effects are markedly Re-number dependant.

Generally these basic initial investigations have shown a very complex forebody flow. They will be followed by further work to improve current knowledge concerning the flow problems involved.

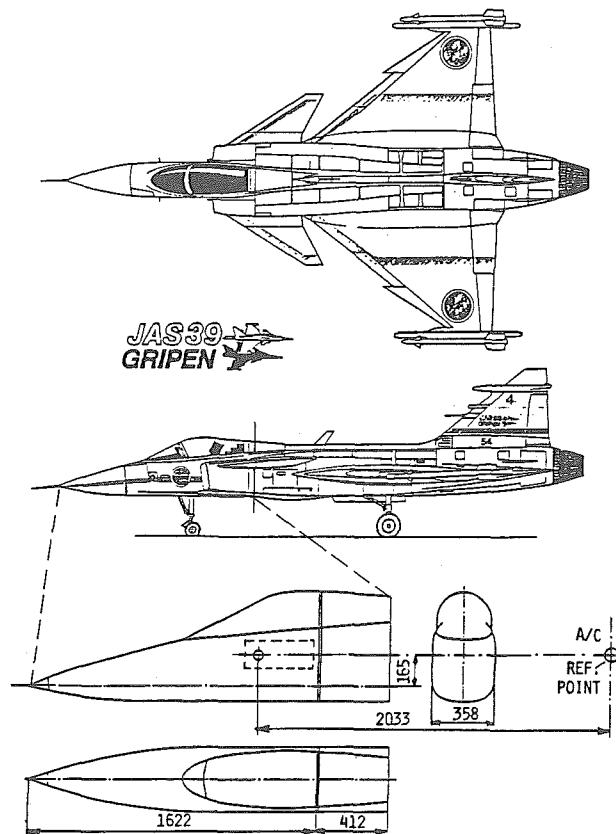


Figure 1. The part-model size compared to the actual aircraft.

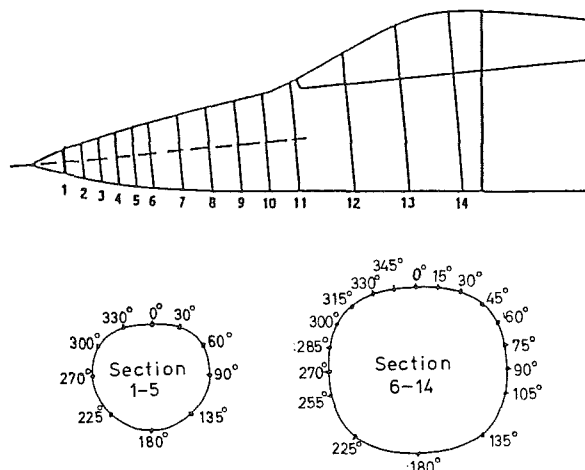


Figure 2. The pressure tappings on the forebody.

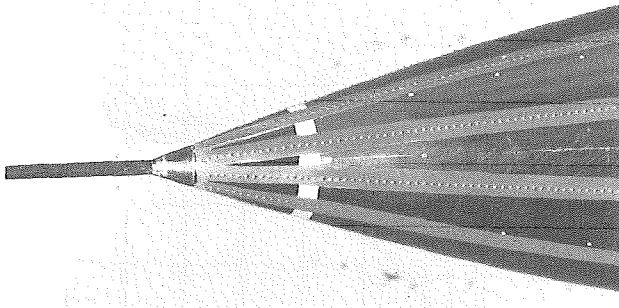


Figure 3. Some of the ten transition trip rows.

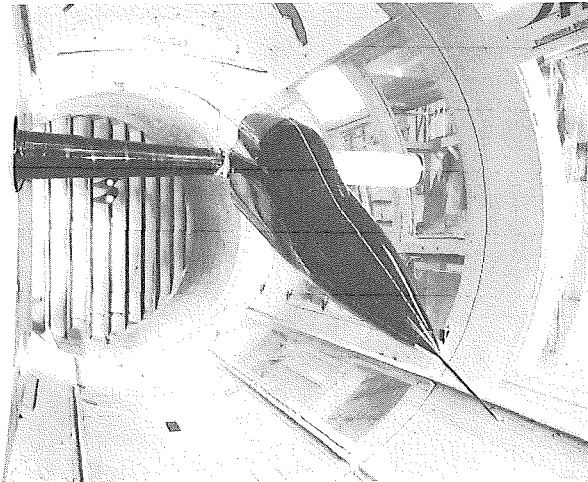


Figure 4. The large part-model in the low speed wind tunnel.

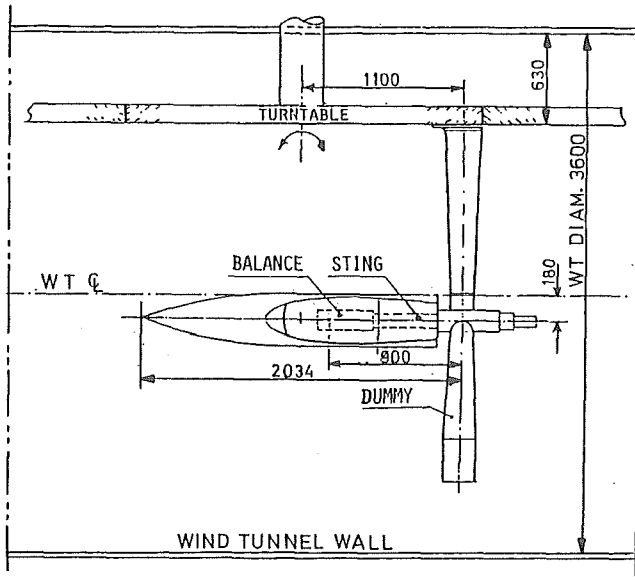


Figure 5. The wind tunnel test section with the large part-model in the high- α rig.




Conf 1		Basic Conf. Bare cone
2		Conf. 1 with pitot-tube
3, 4		3. Short horizontal strakes 4. Without star-board strakes

Figure 6. The four configurations tested.

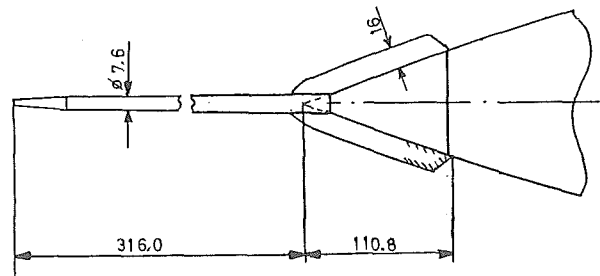


Figure 7. The dimensions of the pitot-tube and the strakes.

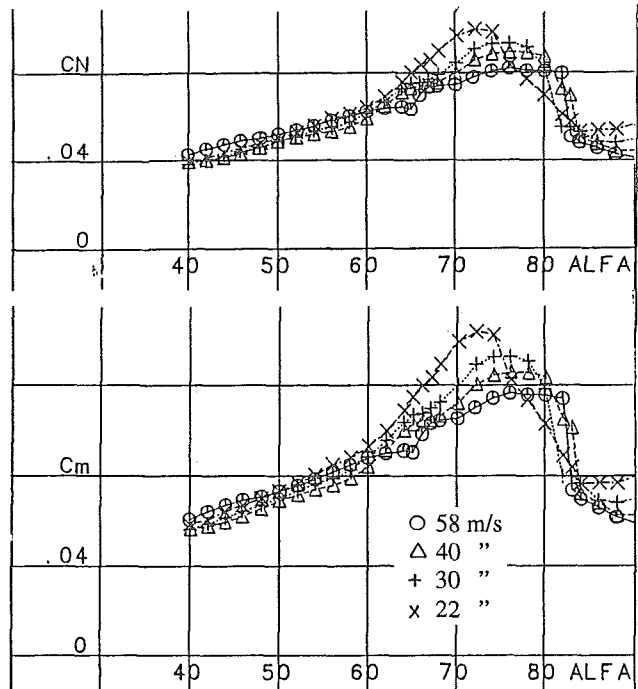


Figure 8. Conf. 1. α -series in the velocity range 22 to 58 m/s.

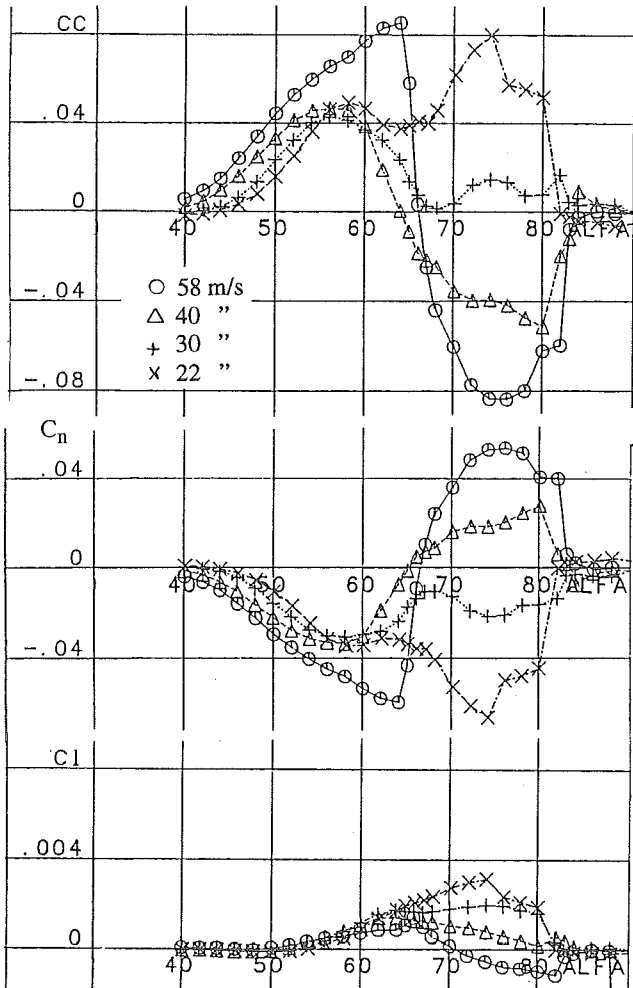


Figure 8. (Cont.)

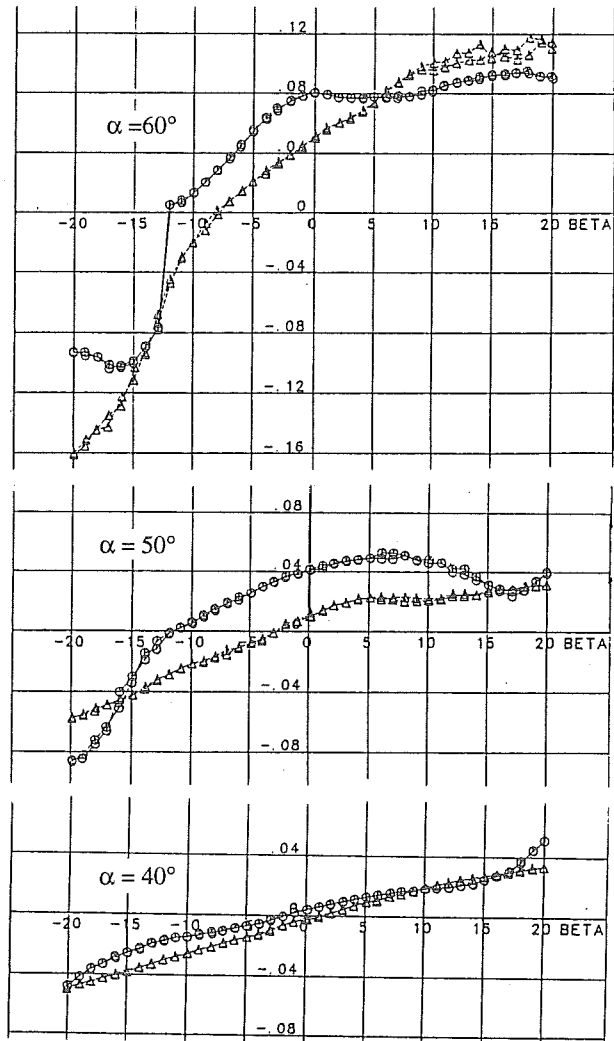


Figure 9. (Cont.)

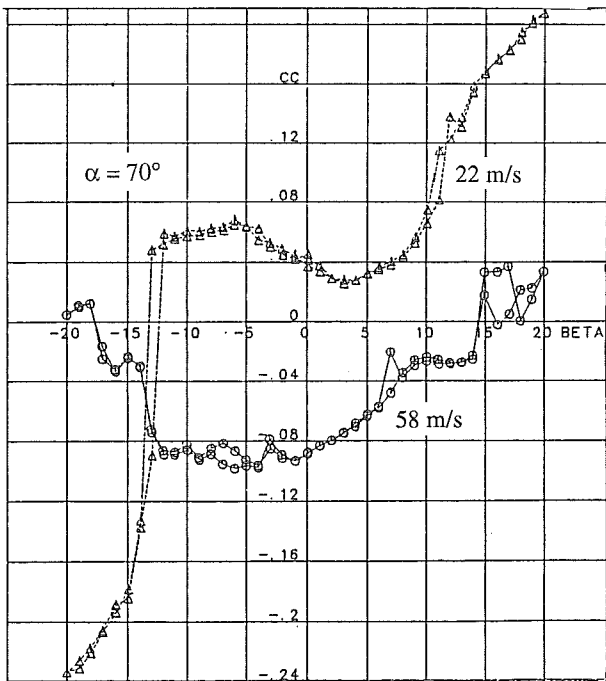


Figure 9. Conf. 1. β -series at 22 and 58 m/s.

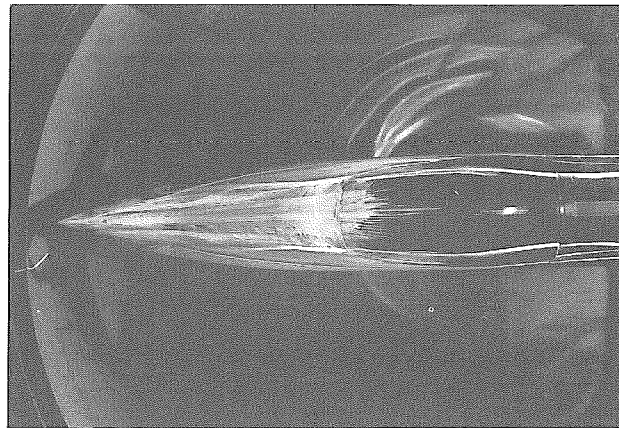


Figure 10. Conf. 1. Oil flow tests at $\alpha = 40^\circ$, 58 m/s.

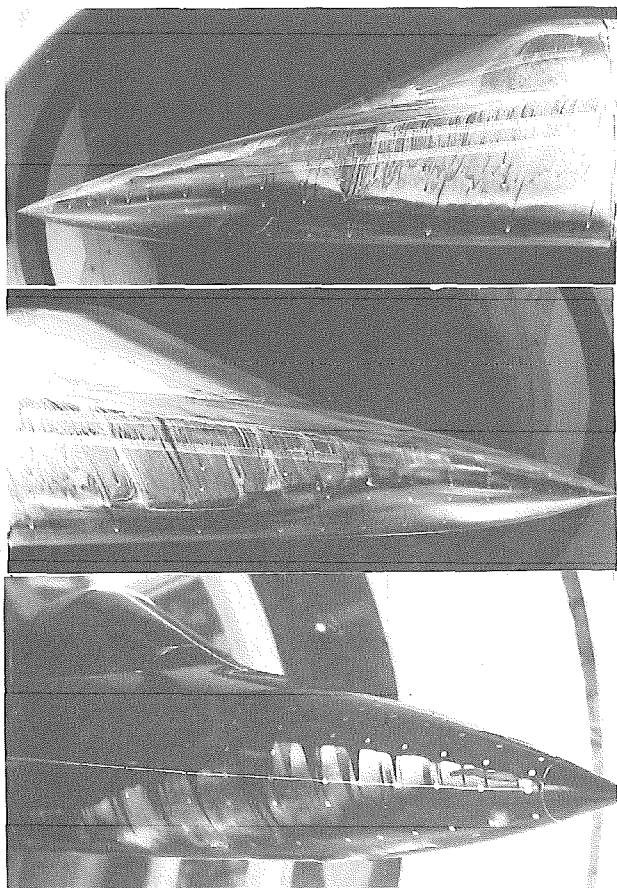


Figure 11. Conf 1. Oil flow and evaporation (lower) tests at $\alpha=62^\circ$, 58 m/s.

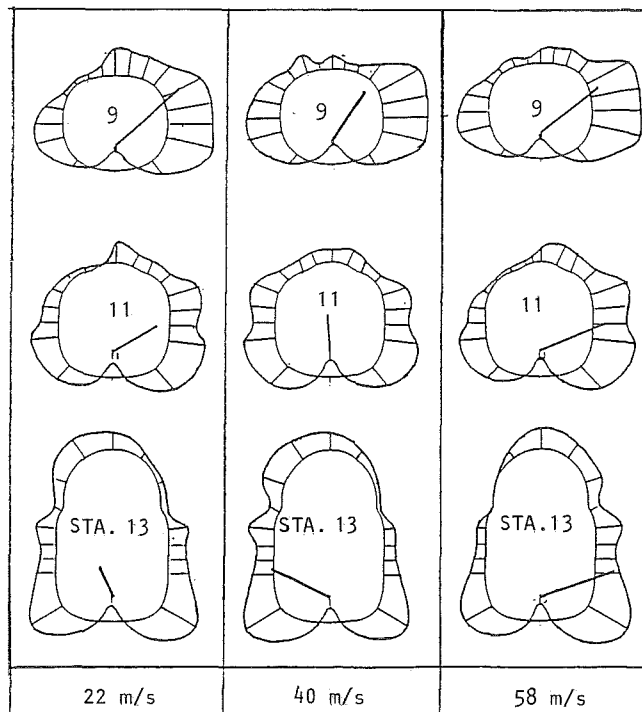


Figure 12. (Cont.)

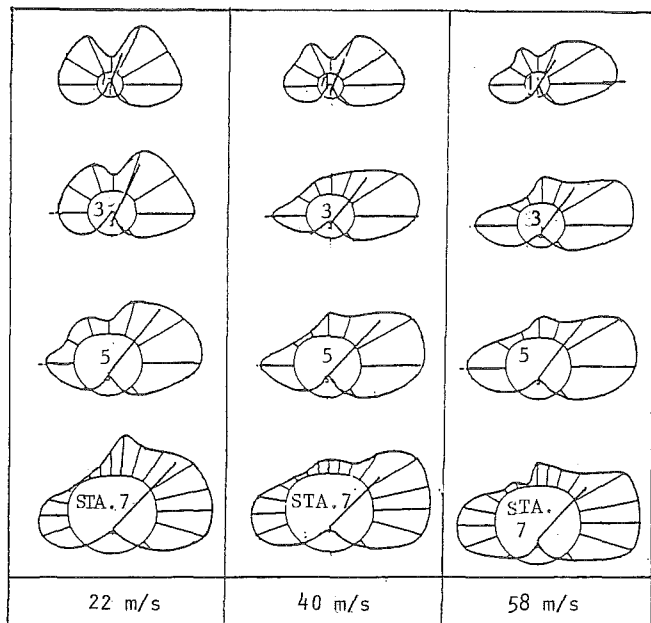


Figure 12. Conf 1. $\alpha=62^\circ$. Pressure distributions at 22, 40 and 58 m/s. (Looking aft.)

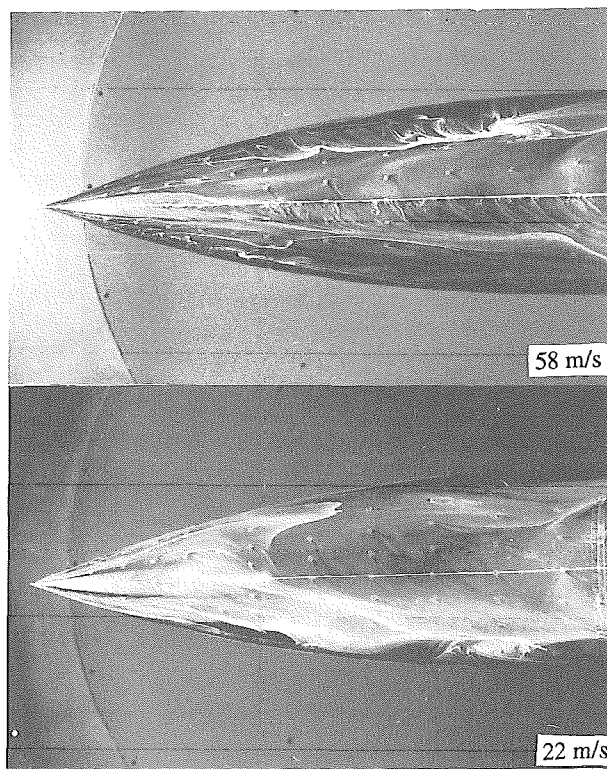


Figure 13. Conf. 1. $\beta=76^\circ$. Oil flow tests at 22 and 58 m/s.

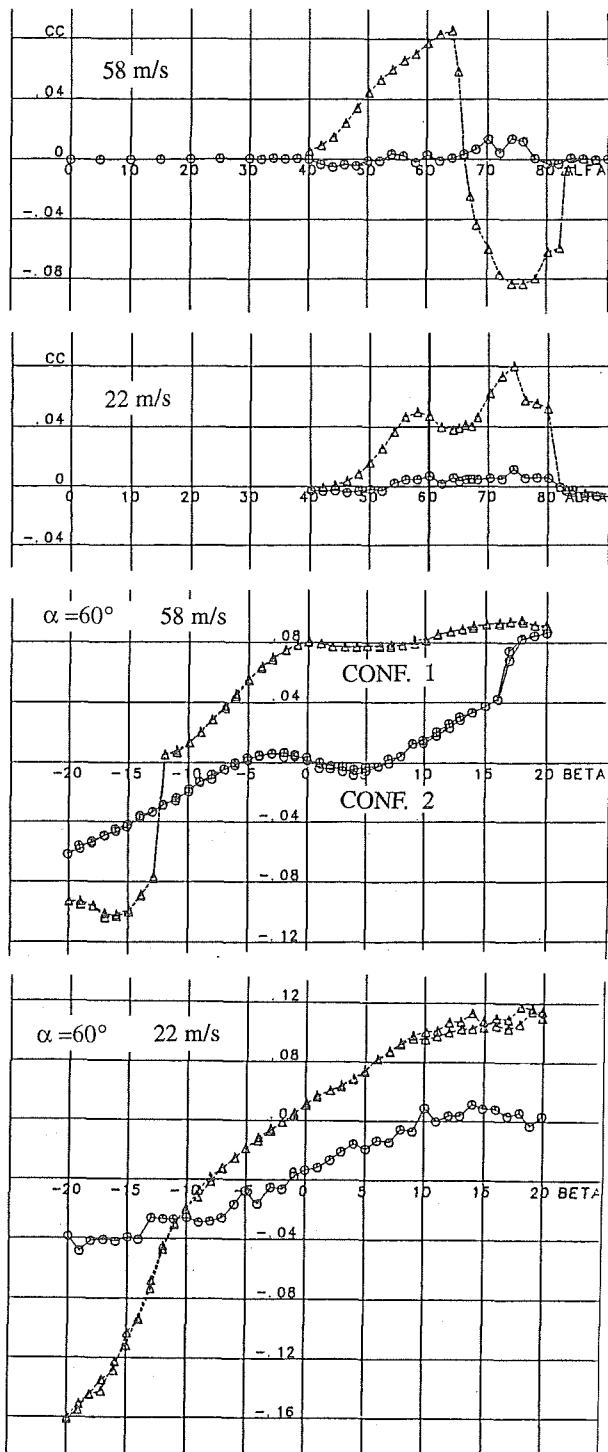


Figure 14. Conf. 1 and 2. The effects of the pitot-tube. α - and β -series at 22 and 58 m/s.

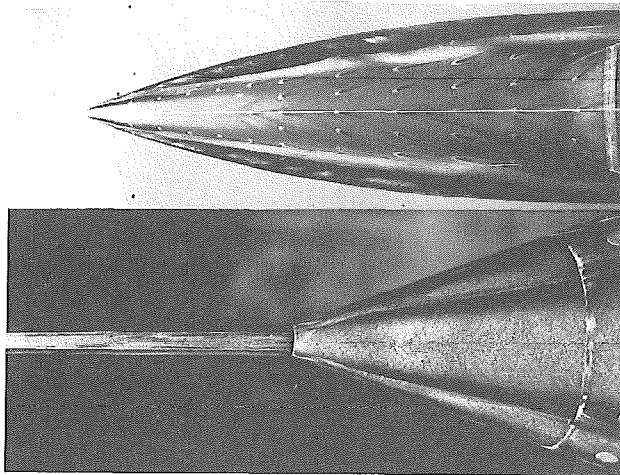


Figure 15. Conf. 2. Oil flow tests at $\alpha = 55^\circ$ and 58 m/s.

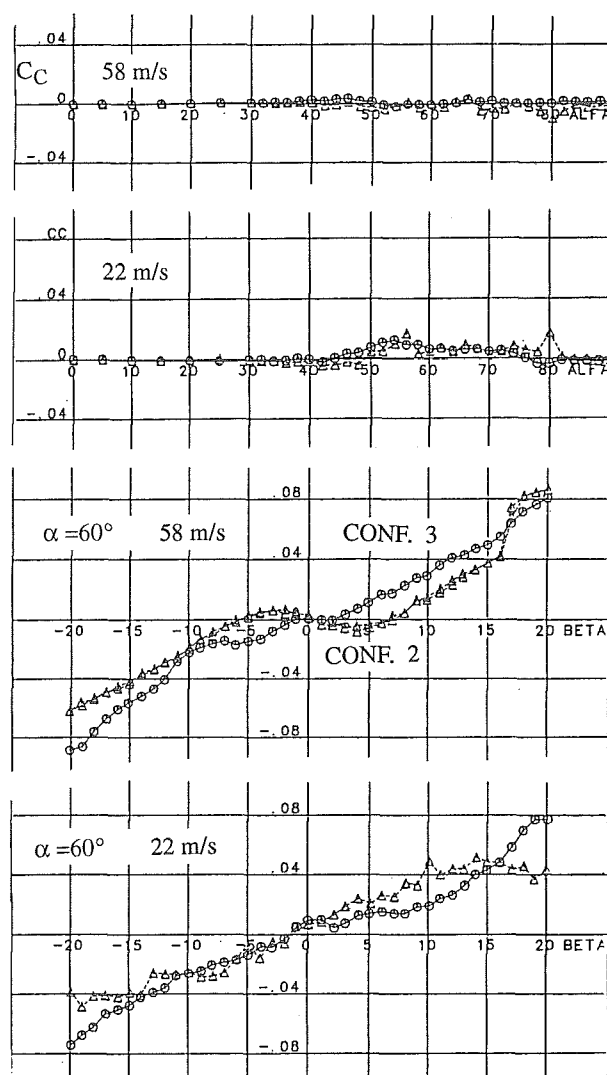


Figure 16. Conf. 2 and 3. The effects of the strakes. α - and β -series at 22 and 58 m/s.

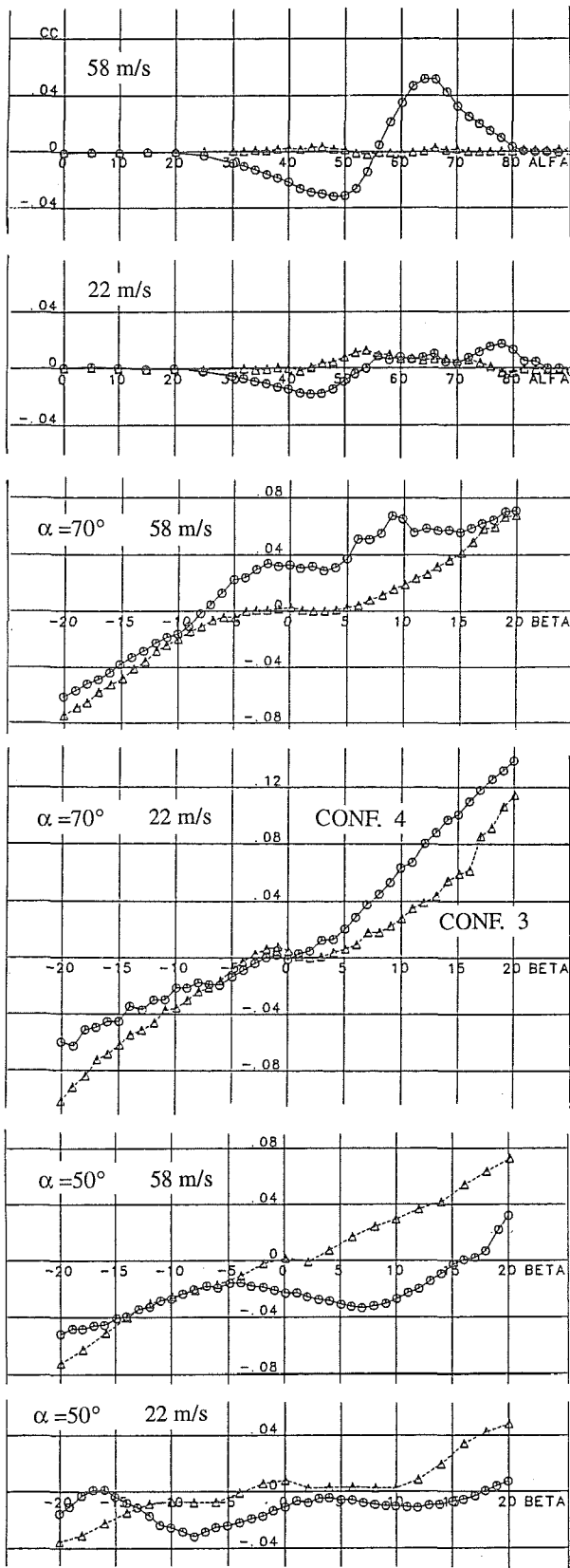


Figure 17. Conf. 3 and 4. The effects of the retraction of starboard strake. α - and β -series at 22 and 58 m/s.

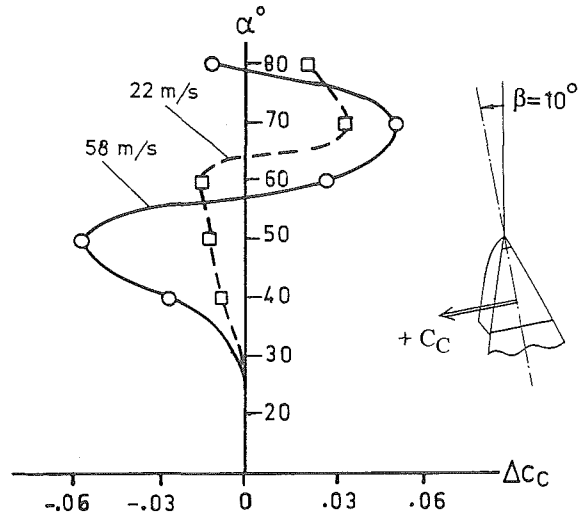


Figure 18. The returning sideforce available when retracting the starboard strake at a $\beta = 10^\circ$ sideslip condition. 22 and 58 m/s.

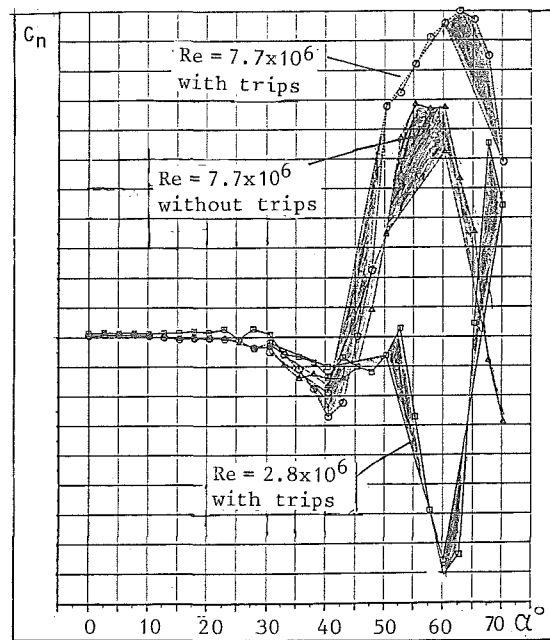


Figure 19. Yawing moment from full-model tests at two Re-number.

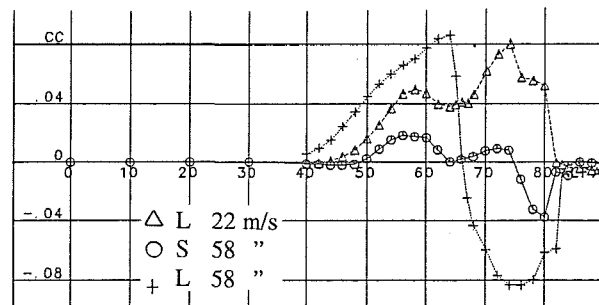


Figure 20. Conf. 1. Comparisons between the large and the small part-models at 22 and 58 m/s.

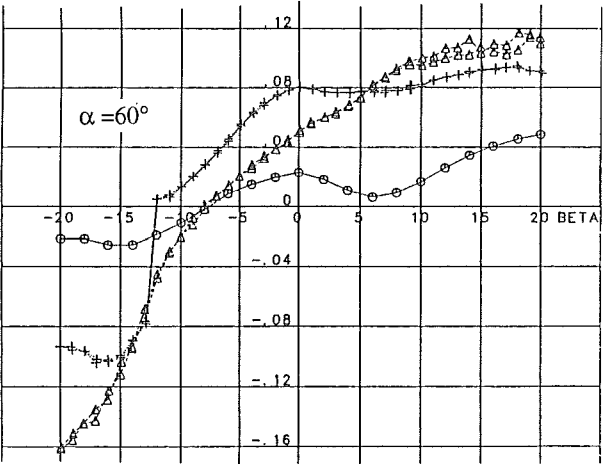
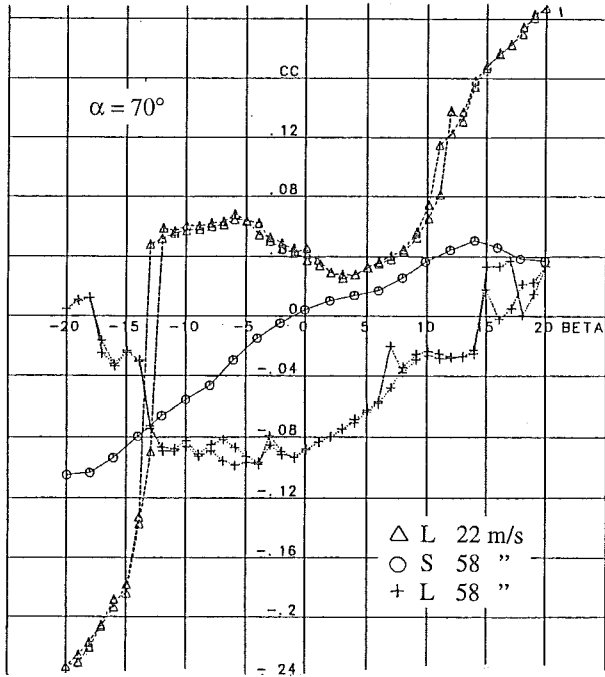


Figure 20. (Cont.)

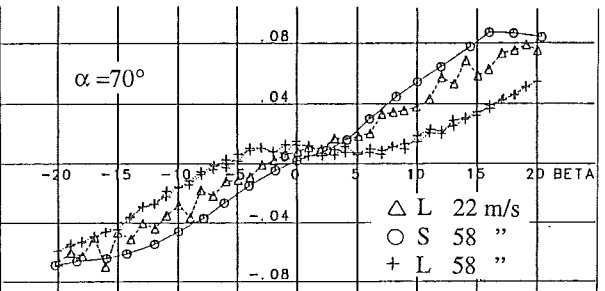
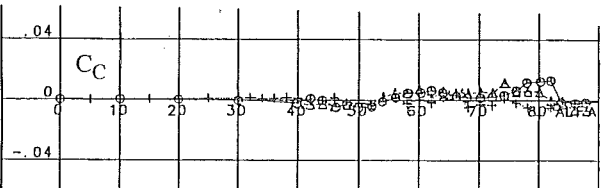


Figure 21. Conf. 2. Comparisons between the large and the small part-models at 22 and 58 m/s.

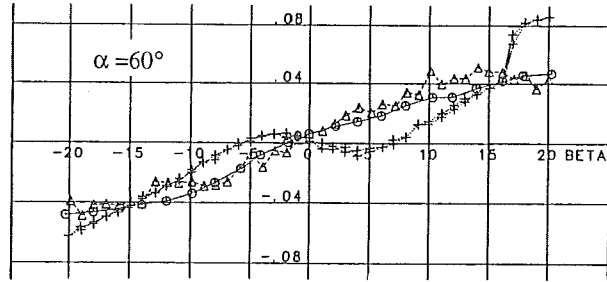


Figure 21. (Cont.)

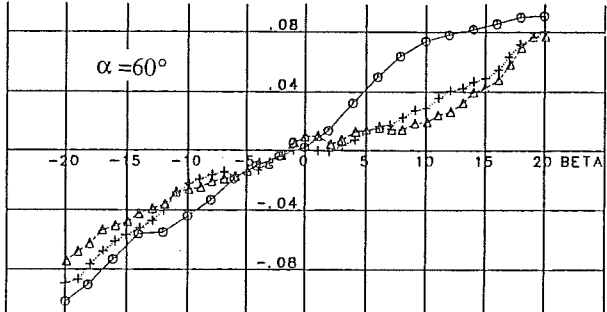
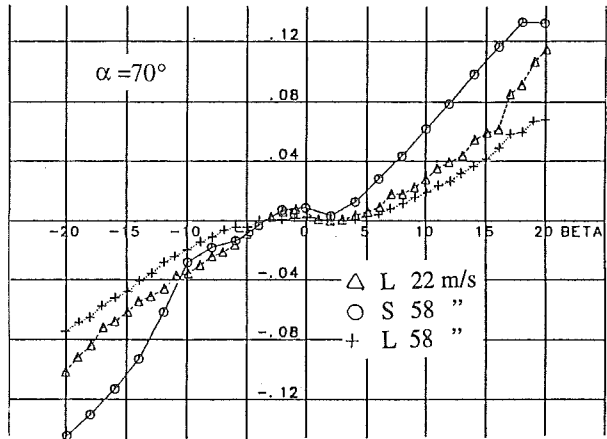
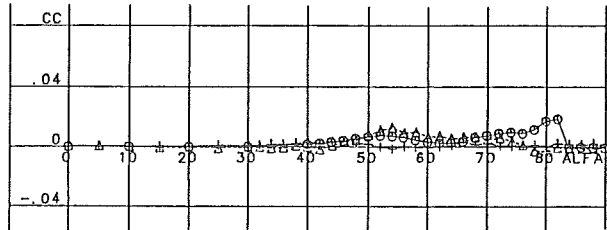


Figure 22. Conf. 3. Comparisons between the large and the small part-models at 22 and 58 m/s.

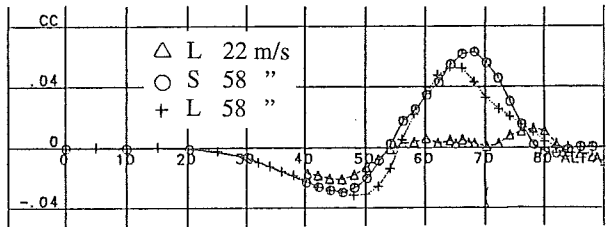


Figure 23. Conf. 4. Comparisons between the large and the small part-models at 22 and 58 m/s.

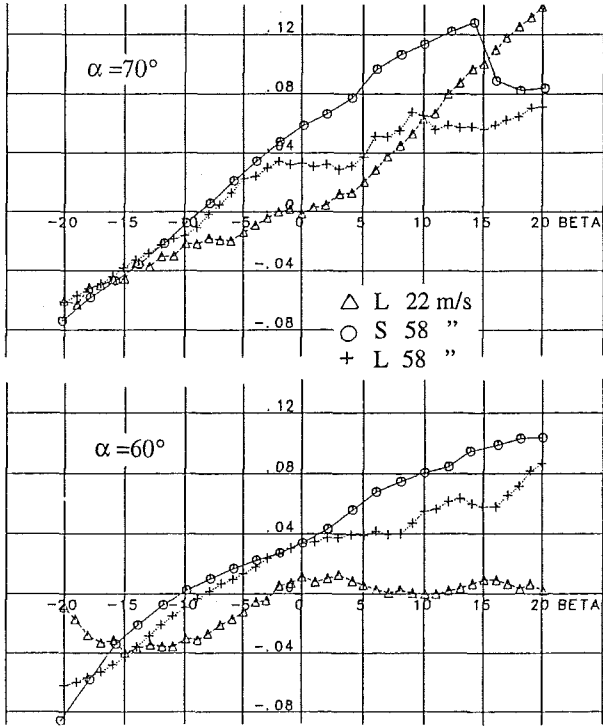


Figure 23. (Cont.)

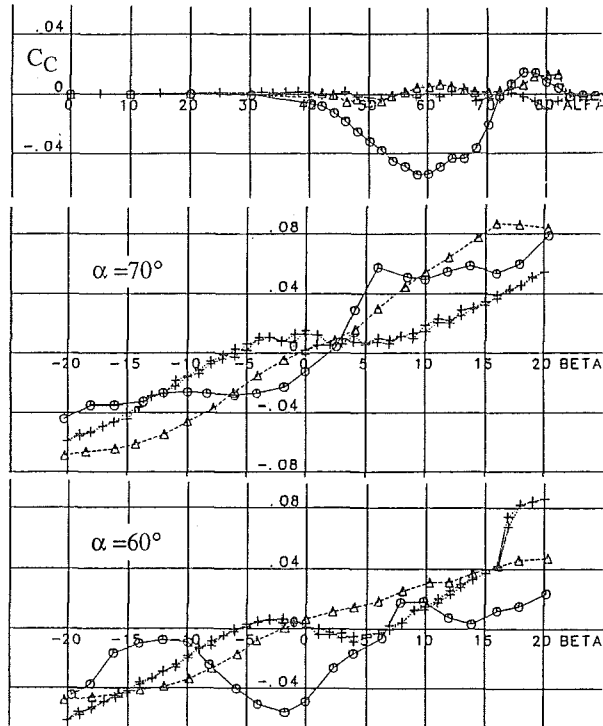


Figure 25. Conf. 2. The effects of transition trips.

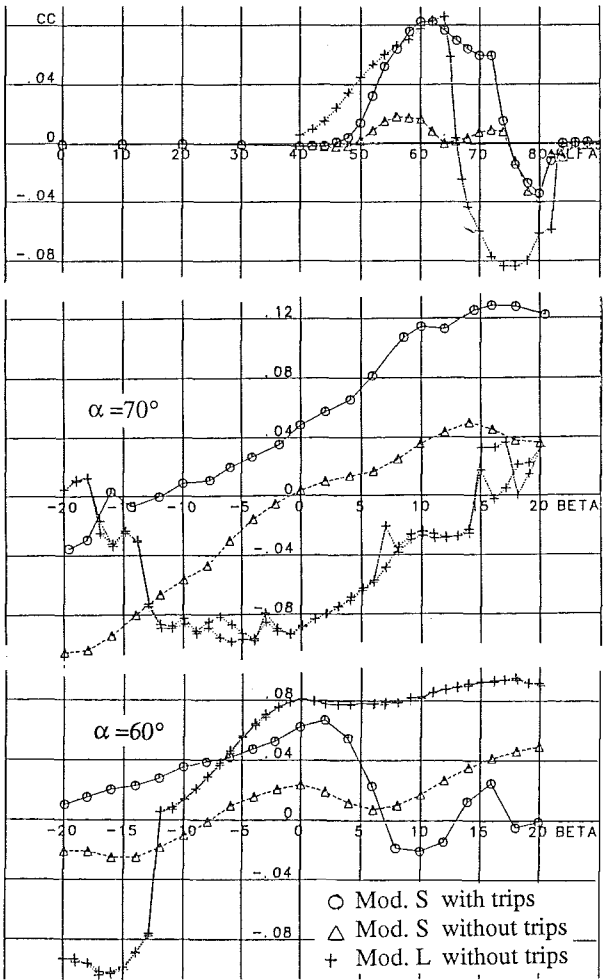


Figure 24. Conf. 1. The effects of transition trips.

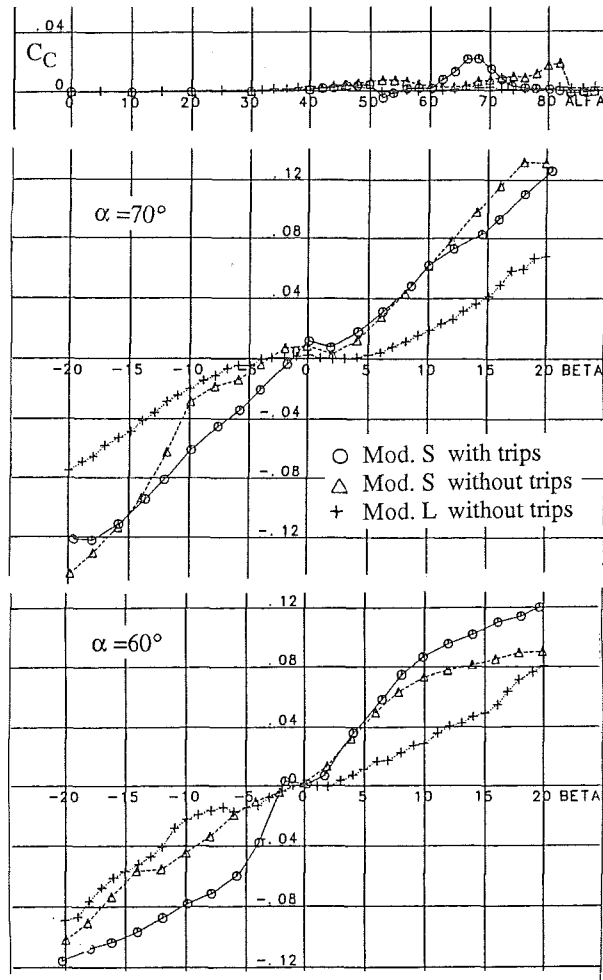


Figure 26. Conf. 3. The effects of transition trips.